In situ voltammetric de-alloying of fuel cell catalyst electrode layer: A combined scanning electron microscope/electron probe micro-analysis study

Ratndeep Srivastava, Prasanna Mani, Peter Strasser[*]

Department of Chemical & Biomolecular Engineering, University of Houston, Houston, TX 77204-4004, USA

ABSTRACT

In situ voltammetric de-alloying, i.e. partial selective dissolution of less noble alloy components, is a recently proposed, effective strategy to prepare active electrocatalysts for the oxygen reduction reaction (ORR) [S. Koh, P. Strasser, J. Am. Chem. Soc. 129 (2007) 12624–12625; R. Srivastava, P. Mani, N. Hahn, P. Strasser, Angew. Chem. Int. Ed. 46 (2007) 8988–8991]. However, in situ de-alloying of bimetallics inside electrode layers of membrane-electrode-assemblies (MEAs) seems to defy the requirement of keeping the membrane free of cationic contaminants; yet, when followed by ion exchange, de-alloyed cathodes result in previously unachieved single cell activities of polymer electrolyte membrane fuel cell cathode layers of up to 0.4 A mg$_{Pt}^{-1}$ at 900 mV cell voltage. The effects of voltammetric Cu de-alloying on the MEA have never been studied before. In the present study, we therefore address this issue and report detailed scanning electron microscope (SEM) imaging of the morphology and electron probe micro-analysis (EPMA) mapping of a MEA at various stages of the de-alloying and ion-exchange process. We investigate the significant loss of Cu from the cathode particle catalyst after de-alloying, demonstrate how the membrane can be cleaned from Cu-ion contamination using ion exchange with protons from liquid inorganic acids, and show that Cu ion exchange does ultimately not affect the activated catalyst particles inside the cathode layer. We correlate the microscopic study of the MEA with its cyclic voltammetric response curves as well as the single cell polarization data.

© 2008 Elsevier B.V. All rights reserved.

1. Introduction

The lack of active, cost-effective and durable electrocatalytic materials for the electroreduction of molecular oxygen (oxygen reduction reaction, ORR) in acidic media is a major scientific obstacle to progress in the development of viable polymer electrolyte membrane fuel cell (PEMFC) technology [3]. The low surface electrocatalytic reaction rates on pure metal surfaces, the most favorable being Pt, cause serious activation overpotentials resulting in intolerable power losses [4]. Pt-rich bulk alloys, such as Pt$_3$Co, Pt$_3$Fe, or Pt$_3$Ni, have shown improved ORR reactivities in both smooth and high surface area (particles) formats [5–13]; yet, the achieved Pt mass-based activities of a factor of 2–3× are still not sufficient for acceptable cost-efficiency [4].

Over the last decade, two electrocatalyst concepts with significantly superior ORR activity have emerged. First, "Pt monolayer catalysts" [14–18] have shown comparable surface area-based current densities at much reduced Pt loadings compared to pure Pt.

Being only at the surface of the catalyst, the dispersion of Pt atoms, that is, the ratio between surface Pt atoms and total Pt atoms approaches one. Hence, Pt monolayer catalysts in a high surface area format (nanoparticles) exhibit much enhanced Pt mass-based activities of up a factor of 10–20×. The Pt monolayer, however, is typically deposited on another noble metal, such as Pd. This reduces the overall noble metal mass-based reactivity to values of 3–4× compared to pure Pt [14,15,19,20]. Second, annealed Pt$_3$Ni(1 1 1) single crystal surfaces have shown impressive improvements of the surface area-based ORR reactivity [21,22]. The enhancement mechanism relies on the formation of a Pt monolayer by surface segregation during the annealing process. The Pt monolayer, referred to as "Pt skin" [5,21,22] is supported on a Pt–Ni alloy bulk and is modified in its electronic properties. Only the segregated Pt$_3$Ni(1 1 1) appears to show the high catalytic activities. Therefore, it is unclear at this point how this concept will be implemented in a high surface area particle-based catalyst concept.

Our group has recently introduced a new paradigm in the preparation of active ORR electrocatalysts. In a series of articles [1,2,23–29], we reported on the strategy of "Voltammetric de-alloying" of base metal-rich bi- and trimetallic alloy nanoparticles, such as Pt–Cu and Pt–Cu–Co. De-alloying referred to the partial, selective electrochemical dissolution of the less noble compo-

---

  * Corresponding author. Current address: Institut fuer Chemie, Technische Universitaet Berlin, 10623 Berlin, Germany. Tel.: +49 30 314 29542; fax: +49 30 314 22261.
    E-mail address: pstrasser@uh.edu (P. Strasser).

nent(s), that is, Cu and Co atoms, resulting in Pt-enriched active alloy nanoparticle catalysts. These active catalysts exhibit 4–6 times higher Pt mass-based ORR activity at 0.9 V/RHE compared to pure Pt nanoparticles.

In case of Pt–Cu bimetallic precursors, compositional and structural analysis of the active catalyst phase has revealed that during the de-alloying process a Pt-rich particle shell is formed surrounding a base metal rich particle core (Pt alloy core–Pt shell catalysts) [1]. Recent experimental evidence points primarily to geometric effects to account for the activity enhancement: the Pt shell of the de-alloyed particles exhibits compressive lattice strain due to the underlying Cu-rich alloy core with shortened lattice parameter [30]. Density functional theory (DFT) studies have predicted that compressively strained Pt surfaces exhibit reduced chemisorption energies of ORR intermediates such as O and OH. The ORR reactivity would therefore be higher on strained Pt shells consistent with experimental observations.

A major step forward toward turning the strategy of "voltammetric de-alloying of nanoparticles" into a viable catalyst concept for PEMFCs consisted on the development of a methodology to implement de-alloyed catalyst into membrane electrode assembly layers. Our group has reported a method to activate alloy nanoparticle precursors "in situ", i.e. inside the electrode layer of a single MEA, using repeated voltammetric cycling for de-alloying [2,25], followed by an ion-exchange step in order to remove excess Cu ions inside the membrane. We showed that using this in situ de-alloying of cathode layers, single cell activities could be achieved comparable to those achieved in rotating disk electrode (RDE) results [1,29] reported earlier. However, detailed information on the fate of the dissolved Cu ions inside the MEA during in situ voltammetric de-alloying and subsequent Cu ion exchange have not been reported to date. Also, to the best of our knowledge, our approach of deliberate contamination of a MEA by leached base metal is unprecedented and unique such that no earlier literature exists on this topic.

To better understand the in situ de-alloying process, we study here the compositional and morphological changes inside an MEA that occur during in situ de-alloying of Pt–Cu alloy catalysts. We study structural characteristics of the catalyst material as well as voltammetric responses of the single PEMFC cell before and after de-alloying. We observe the formation of metallic Cu bands inside the membrane and demonstrate the feasibility of the in situ de-alloying method to activate MEAs.

2. Experimental

2.1. Preparation of electrocatalysts

Carbon-supported Pt–Cu alloy was prepared using the liquid-based impregnation method. It was synthesized by adding appropriate amounts of solid Cu precursor ($Cu(NO_3)_2 \cdot 6H_2O$, Sigma–Aldrich #239267) to a commercial powdered electrocatalyst consisting of about 30 wt% platinum supported on a high-surface area carbon support (TKK-based). De-ionized water (>18.2 MΩ, Millipore Gradient System) was added to the supported catalyst powder and the mixture was sonicated for 45 min (Model 75D, VWR) until a thick slurry formed. The catalyst slurry was subsequently frozen in liquid nitrogen until and then freeze-dried in vacuum (50 mTorr) overnight until room temperature is achieved. The resulting catalyst precursor powder was distributed evenly into two small ceramic crucibles. The crucibles were then placed in the center of a 3 ft long quartz tube (3 in. diameter) flow furnace (Lindberg Blue). The powder was then annealed to a maximum temperature of 600 °C for 7 h (10 K min^{-1} heating rate) under a flowing 6% hydrogen atmosphere (Ar balance) and subsequently slowly cooled down without any forced convection.

2.2. Membrane cleaning

Nafion® NRE212 membrane obtained from Dupont was cut into several 17 cm × 20 cm pieces and washed with de-ionized (DI) water at 80 °C for 1 h twice. Glass rods were kept at the surface of the trough while boiling to avoid excessive heating of the membrane. After treating the membranes with DI water they were heated at 80 °C with 5 wt% H_2O_2 for 1 h. They were further washed with DI water at 80 °C twice to remove any H_2O_2 left. The treatment with H_2O_2 is to facilitate the removal of dirt from the membrane. Following peroxide treatment they were washed with 1 M sulfuric acid for 1 h at 80 °C. This helps in removal of metallic impurities from the membrane. Further to remove any trapped acid from the membrane it is twice washed with DI water at 80 °C for 1 h. We repeat the above step again to ensure complete removal of sulfuric acid. Finally the pH of the discarded water is measured to check the neutrality of the solution The treated membrane is stored in DI water for further use.

2.3. Catalyst ink preparation

We measure catalyst powder between 0.1–0.15 g. To this 2–3 drops of DI water were added to avoid catalyst burning after addition of solvent in the next step. The slurry obtained is mixed with pre-refrigerated iso-propanol (10–15 min refrigeration), the amount is 33 vol.% (in L) of the catalyst weight. The solution is stirred continuously for 15 min with a magnetic stirrer. Thereafter the solution is sonicated for 1 h, followed by addition of 33 wt% Nafion (5 wt%, DE 521) with further sonication of 1 h.

2.4. Membrane-electrode-assembly preparation

The Pt–Cu alloy nanoparticle precursor was coated with constant geometric Pt loading ∼0.1 mg$_{Pt}$ cm^{-2}$_{geo}$ on the cathode, while a commercial 40 wt% Pt/C catalyst was deposited on anode (Pt loading = 0.2 mg$_{Pt}$ cm^{-2}$_{geo}$). Catalyst coating is obtained using an automated three-axis robotic dispensing machine obtained from PVA Inc. (Precision Valve Automatics, Albany). The FCS 100 ES spray valve® (PVA Inc.) was used to produce uniform concentrated atomized coating film on the membrane. The arm was controlled via a computer using a RS 232 interface and PathMaster® software. The ink as prepared above was transferred to the spraying nozzle using a peristaltic pump (Masterflex®, Cole-Parmer Inc.).

Ink spraying was done at 5 psi atomizing pressure (N_2 was used as atomizing gas) and 0.05 ml min^{-1} ink flow rate. These conditions were found to be optimum from various sets of MEA preparations done earlier.

20 cm^2 Nafion NRE212 membrane piece was dried using N_2. It was held between a substrate with a window opening of 10 cm^2 to make an area of coated catalyst. A pre-weighed 9 cm^2 carbon paper from SGL was fixed in the path of the spray to act as a reference. The carbon paper was weighed frequently to determine the loading on the membrane. MEA was dried with the substrate for at least 12 h at 80 °C at the end of the coating.

2.5. Electrochemical de-alloying

A 10 cm^2 cell assembly (flow plates, metal contacts) was designated for electrochemical de-alloying procedures, since base metal dissolution contaminates the flow fields after repetitive de-alloying. We also diverted the outlet vent lines from the single cell through stainless steel bottles to collect Cu-ion contaminated water excess water.

After MEA preparation, the single cell was assembled using a gas diffusion media (GDM) GDL 10BC (SGL Carbon Inc.). To record the initial cyclic voltammogram (CV) of the precursor cathode materials, the cell temperature was fixed at 30 °C, whereas cathode and anode humidifier are kept at 50 °C (slightly over humidified conditions). Humidified hydrogen and nitrogen are fed on the anode and cathode, respectively, at flow rate of about 160 sccm. This flow was constant during the de-alloying procedure. After stabilization of the open-circuit potential (OCP), a CV was measured using an external potentiostat (GAMRY reference 600) with the cathode layer being the working electrode. The potential was swept between 0.05 V and 1.2 V at a scan rate of 20 mV s^{-1}. Now the cell temperature was increased to 80 °C and cathode and anode humidifier temperature was raised to 80 °C (=100% relative humidity, RH). Cathode feed is switched to pure oxygen and the cell is put into the potentiostatic mode (AMREL electronic load, supplied by Fuel Cell Technologies, Inc., Albuquerque) at a constant voltage of 0.6 V. In this condition, the cell is allowed to hydrate for about 4 h. Thereafter, the cell temperature is brought down again to 30 °C, and cathode and anode humidifying temperatures are set at 50 °C. Nitrogen is fed on the cathode and *in situ voltammetric* (*electrochemical*) *leaching* is started. De-alloying was achieved by repeated cycling (200–300 cycles) at 100 mV s^{-1} between 0.5 V and 1.0 V until the hydrogen adsorption and desorption peaks became time-stable and similar in shape to a clean Pt surface. Thereafter, a CV was re-measured in the 0.05–1.2 V potential range to characterize the Pt surface area at this point of the de-alloying procedure.

The cell was now disassembled and the MEA was removed and washed in 1 M sulfuric acid at 80 °C for 1 h, followed by repeated washing with DI water to remove SO_4^{-2} ions in the MEA. The MEA was then dried in an air oven at 80 °C overnight.

2.6. Fuel cell testing

The electrochemically de-alloyed MEA with active area of 10 cm^2 was assembled with gas diffusion media, GDL 10BC (Sigracet®, SGL Carbon Inc.), 3-channel serpentine flow fields (Poco® graphite blocks) and gold-coated current collectors supplied from Fuel Cell Technologies Inc. It was held at a compression of 75 in-lb with a digital torque range (ComputorQ3, CDI torque) and tested in a dual channel test station (Fuel Cell Technologies Inc., Albuquerque). For performance testing and polarization curve measurements, the RH of both feed streams were kept at 100%, with $T_{CELL} = 80$ °C. The MEA underwent another activation at 150 kPa$_{abs}$ pressure under potentiostatic conditions (0.6 V cell voltage) for 4 h in H$_2$/O$_2$ at 2/9.5 stoic. Once the current stabilized, the MEA was then further conditioned for 24 h galvanostatically at the current recorded at 0.6 V under H$_2$/O$_2$, at 2/9.5 stoic at 150 kPa at 100% humidity. Finally, polarization curves (*E–I* curves) were recorded using LabView® control software. During *E–I* measurements, stoichiometric flows of $\lambda = 2/9.5$ (H$_2$/O$_2$) for $i \geq 0.2$ and 0.2 A cm^{-2} flows for $i < 0.2$ A cm^{-2} were maintained. IR correction was achieved by correcting the cell voltage by the experimental ohmic resistance of the cell probed by an AC impedance analyzer. The frequency of the AC impedance analyzer sine waves was set to 1 kHz and the peak-to-peak amplitude of the fuel cell was optimized to be 50 mA in the entire range of the fuel cell DC to reduce noise/harmonics.

2.7. Electrochemical surface area characterization

Pt surface area was determined by CV measurements with the anode and cathode fed with H$_2$ and N$_2$, respectively. The cell temperature was kept at 30 °C, humidifiers at 50 °C and at atmospheric pressure. Cyclic voltammogram are performed between 0.05 V and
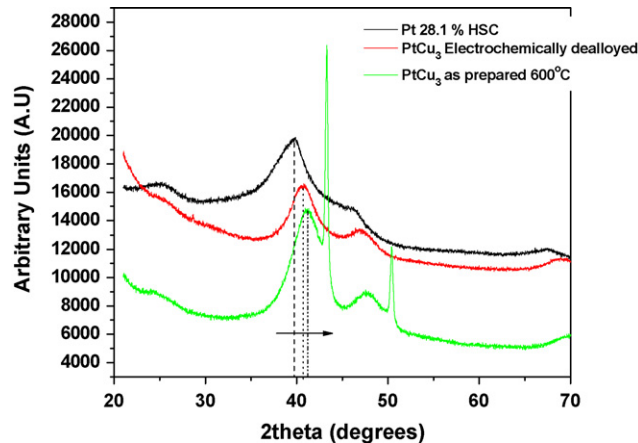
Fig. 1. X-ray diffraction profiles of the high-surface area carbon (HSC)-supported pure Pt synthesis precursor (black), the as-prepared Pt$_{25}$Cu$_{75}$ catalyst precursor (green) and the de-alloyed active Pt–Cu cathode catalyst (red). Synthesis condition 600 °C, 7 h annealing in 6% H$_2$/Ar. The arrow indicates a shift in the fundamental (1 1 1) peak position with alloying reflecting a contraction of the lattice parameter. (For interpretation of the references to color in this figure legend, the reader is referred to the web version of the article.)

1.2 V at a scan rate of 20 mV s^{-1}, the area of H$_2$ adsorption peak between 0.05 V and 0.4 V is calculated after double layer correction using the commonly used conversion factor of 210 µC cm^{-2}.

2.8. Sample preparation for EPMA

Three MEAs were used for elemental mapping. First, an as-prepared MEA (MEA 1), second a de-alloyed MEA (MEA 2), and third, a de-alloyed and ion-exchanged MEA (MEA 3). Small portions of the MEA were cut with a diamond knife and hardened in a epoxy solution overnight. The surface was polished with 1 µm alumina solution for 15 min and then coated with 100 nm thick carbon layer. The sample was put in a JEOL JXA-8600 microprobe.

3. Results and discussion

3.1. Structural changes of the catalyst during de-alloying

Fig. 1 compares the X-ray diffraction profiles of a number of Pt and Pt alloy nanoparticle electrocatalysts: the black profile shows the pure carbon-supported Pt nanoparticle catalysts which was used as starting material for the synthesis of he Pt$_{25}$Cu$_{75}$ precursor material. The green profile shows the as-prepared carbon-supported Pt$_{25}$Cu$_{75}$ precursor alloy material annealed at 600 °C for 7 h [1]. Generally, Pt–Cu alloys form disordered face-centered cubic (fcc) crystal structures [31] characterized by the strong fundamental (1 1 1) reflection and weaker (2 0 0) and (2 2 0), etc. reflections [32]. The Pt–Pt interatomic distance decreases as more and more Cu atoms substitute Pt atoms. Disordered fcc Pt–Cu alloys follow Vegard's law fairly well [33,34]; this implies that the peak position of the (1 1 1) reflection (in the absence of lattice strain) can be used to predict the corresponding alloy composition. For the prepared Pt–Cu alloy precursors of Fig. 1, the (1 1 1) reflection was observed at around $2\theta = 41.8°$ indicating a Cu content in the alloy phase between 60 at.% and 75 at.%. Since the overall Cu content was set to be 75 at.%, some additional Cu must be present. In fact, a non-alloyed, pure Cu fcc phase caused the additional sharp peaks at $2\theta = 43.5°$ and $2\theta = 51°$ in Fig. 1 which are consistent with the (1 1 1) and (2 0 0) fundamental reflections from the ICDD database [31]. The peak width suggests that the pure Cu crystallites are large compared to the alloy phase. Weak and broad reflection at around
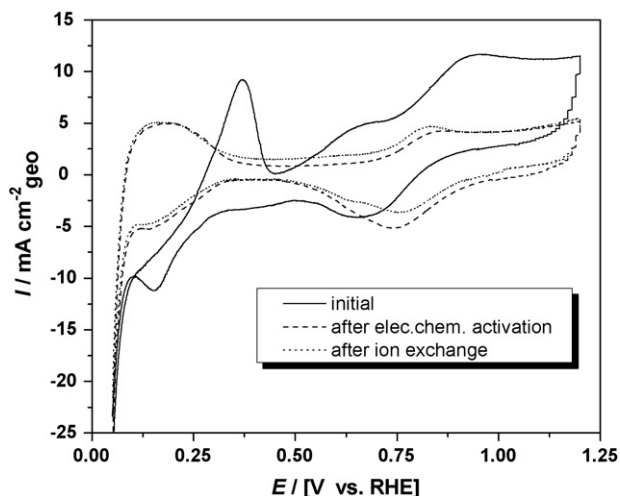
Fig. 2. Cyclic voltammograms (CVs) reflecting the interfacial processes at the cathode layer in a single PEM fuel cell. Initial CV of an as-prepared $Pt_{25}Cu_{75}$ precursor (solid), after electrochemical in situ de-alloying (dashed) and after ion exchange using sulfuric acid (dotted). Condition: H_2/N_2, $T_{cell} = 30\,C$, $T_{hum} = 50\,°C$, $P = 1\,atm$, 0.05–1.2 V, 20 mV s^{-1}, 160 sccm flow on both sides. Taken from Ref. [25].

Fig. 3. Polarization curves (V–I curves) of single fuel cell MEAs employing: (i) a de-alloyed $Pt_{25}Cu_{75}$ cathode catalyst after ion exchange (squares), (ii) a de-alloyed $Pt_{25}Cu_{75}$ cathode catalysts without ion exchange (lower triangles), (iii) a standard 30 wt% Pt/C catalysts (circles) and (iv) a standard 45 wt% Pt/C catalyst (upper triangles). Anode catalyst in all cases was a 40 wt% Pt/C-ETEK Inc. Measurements were taken at 100% RH, $T_{CELL} = 80\,°C$ and 150 kPa. The cell potential was IR corrected and corrected for H_2 cross-over current.

angle $2\theta = 25°$ can be attributed to some crystallinity of the carbon support.

The red profile in Fig. 1 illustrates the structure of the cathode catalyst after de-alloying. The pure Cu reflections have disappeared, and the fundamental (1 1 1) reflection of the Pt–Cu alloy phase has shifted to smaller angles indicating a loss of Cu from the alloy phase. The results are consistent with a severe depletion of metallic crystalline Cu from the cathode catalyst during voltammetric de-alloying. Compositional information cannot be taken from the bottom profile in Fig. 1 since compressive lattice strain may have built up during the de-alloying process which would cause smaller unit cell parameters (smaller Pt interatomic distances) than expected from the alloy phase composition.

3.2. Cyclic voltammetric response of the catalyst during de-alloying

3.2.1. The initial CV

Fig. 2 [25] reports the very initial CV of the cathode electrocatalyst inside a MEA at the beginning of the in situ de-alloying of the cathode catalyst. The sweep was started at 0.05 V/RHE and continued in anodic direction. A negative faradic current indicated the deposition of Cu ions from the cathode layer onto the electrocatalyst. This observation suggests that some Cu must have been already leached out of the Cu-rich precursor during the preparation of the MEA. Cu dissolution from the carbon-supported $Pt_{25}Cu_{75}$ alloy nanoparticle precursor can be explained by mixed open-circuit potentials resulting from the presence of the Cu^{2+}/Cu, the O_2/H_2O, and the H_2/H^+ redox couples in a Nafion^{TM} containing, and therefore acidic medium. Past the Cu^{2+}/Cu redox potential of about +0.34 V/RHE, the initial CV in Fig. 2 displays a strong Cu dissolution peak followed by a broader anodic dissolution feature around 0.6–0.7 V/RHE. We have investigated similar CV profiles during the early stages of Cu dissolution from Pt–Cu bimetallic alloy surface in half-cell arrangements [23]. In that study, we were able to correlate the dissolution peak potentials with the detailed atomic environment (nature and number of coordinating atoms) of the dissolving Cu surface atoms. The anodic peak around 0.34–0.5 V/RHE is related to the dissolution of lower coordinated Cu surface atoms which are largely surrounded by Cu atoms and, therefore, exhibit largely Cu

bulk character. The anodic feature at 0.6–0.7 V/RHE, in contrast, was linked to higher coordinated Cu surface atoms at step edges or kinks and mainly surrounded by Pt atoms [23,35–37]. The resemblance of the voltammetric Cu dissolution profiles under RDE and MEA conditions suggests similar surface processes in the measurements of Fig. 2. On the cathodic sweep of the initial profile, a broad voltammetric feature near 0.6–0.7 V/RHE indicates the re-deposition of Cu on Pt, before Cu bulk deposition sets in below 0.34 V/RHE. At 0.05 V/RHE a sharp increase in cathodic current density indicates the onset of the hydrogen evolution.

The voltammetric in situ de-alloying protocol involved holding a constant cell potential of 0.6 V for 4 h under H_2/O_2 conditions, followed by at least 200 consecutive potential cycles between 0.5 V/RHE and 1.0 V/RHE under H_2/N_2 flow.

3.2.2. CV response after de-alloying

After de-alloying by repeated potential cycling, the initial CV of the cathode layer transformed into the dashed profile of Fig. 2. No sign of Cu dissolution was discernible anymore. Instead, a hydrogen ad/desorption peak indicated the presence of Pt surface atoms. Furthermore, Pt-oxide features became discernible at and above 0.8 V/RHE. Overall, the cathode catalyst profile after Cu de-alloying strongly resembled that of a pure Pt electrocatalyst.

3.2.3. CV after Cu ion exchange

Earlier reports showed that removal of dissolved Cu ions in a half-cell electrode set up using liquid electrolytes [1,29] was not necessary to yield high ORR activity, because the Cu ions diffused into the liquid phase and did not significantly affect the de-alloyed active catalyst. This situation is quite different in an MEA environment where Cu ions get easily trapped at sulphonic groups of the fuel cell membrane. This is why in Refs. [25] and [2], Cu ion exchange by means of strong inorganic acids was used to remove excess Cu ions from the membrane. The dotted profile in Fig. 2 shows the CV of the cathode catalyst after ion exchange. The experimental observation shows that the ion exchange had no detrimental effect on the interfacial profile of the cathode catalyst. In fact, the CV profile is almost identical to that obtained before ion exchange.
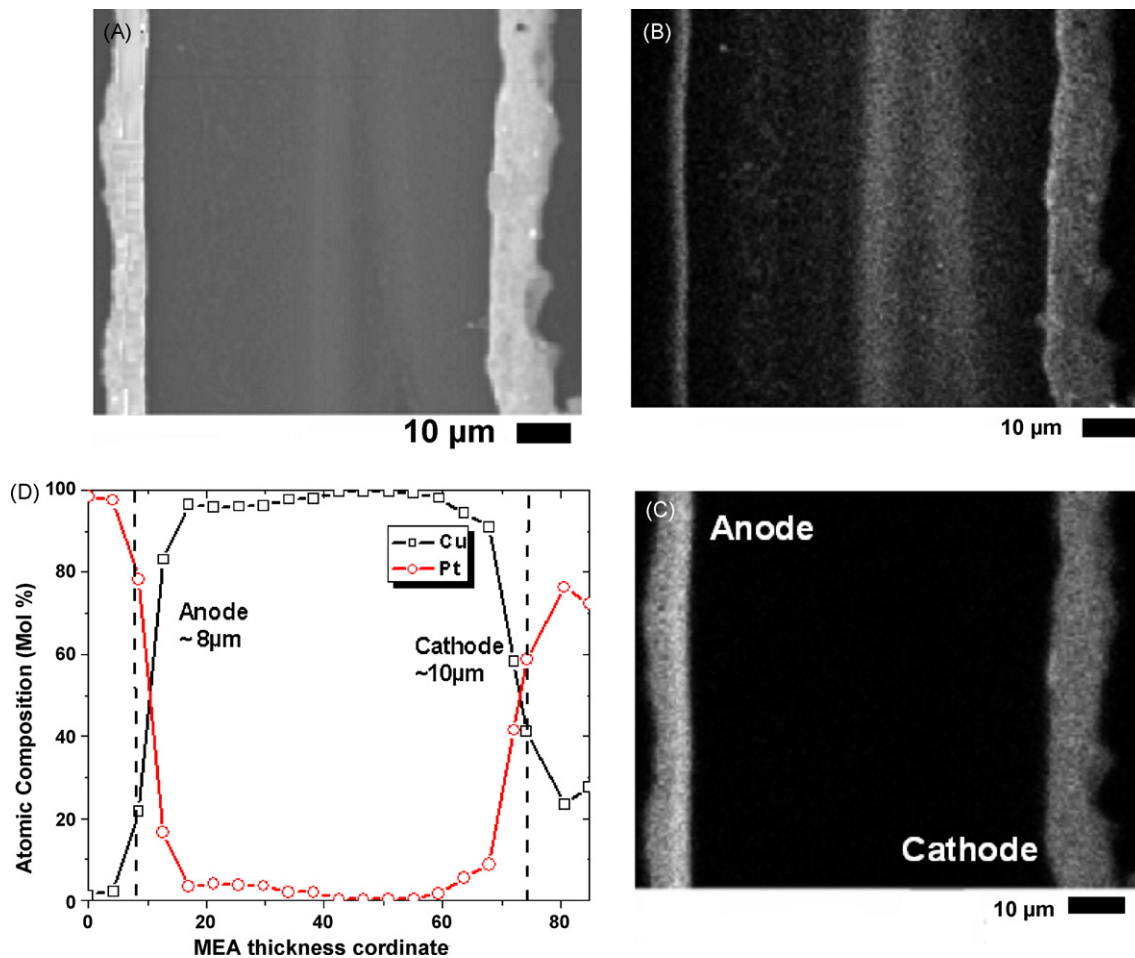
Fig. 4. EPMA mapping of an as-prepared MEA employing a $Pt_{25}Cu_{75}$ catalyst precursor on the cathode and a 40% Pt/C catalyst on the anode. (A) backscattered image of the membrane cross-section, (B) Cu map of the MEA, (C) Pt map of the MEA and (D) atomic composition of PtCu across the MEA. Note that only in the simultaneous presence of Pt and Cu are the compositional values accurate. In the absence of one of the two species, the normalization displays the composition of the respective other as 100%. Catalyst loadings $L_{Pt,Cathode} = 0.2073\,mg_{Pt}\,cm^{-2}$ and $L_{Pt,Anode} = 0.2123\,mg_{Pt}\,cm^{-2}$.

3.3. Performance of de-alloyed Pt–Cu catalysts

The de-alloying of large amount of Cu atoms bears the question where the Cu ions are located after the de-alloying process and how they may affect the MEA behavior. No experiments on the consequences of Cu-ion poisoning of the membrane on MEA performance have been provided to date. To address this, we have performed MEA polarization measurements before and after ion exchange. Fig. 3 reports the IR-corrected as well as cross-over current corrected cell voltages as function of the geometric current densities. Polarization curves recorded immediately after in situ de-alloying of Cu but without ion exchange exhibited catastrophic performance with very small open-circuit potentials, current and power densities (lower triangles in Fig. 3). Visual inspection of this MEA revealed that the membrane had taken on a reddish color, obviously from metallic Cu located inside the membrane. It became clear that removal of Cu ions after de-alloying is crucial in order to fully unfold the potential of the de-alloyed catalysts.

The de-alloyed and ion-exchanged MEAs (squares in Fig. 3) showed a significantly improved polarization behavior compared to standard 30 wt% (circles) and 45 wt% Pt/C (upper triangles) cathode catalysts. Cathode electrode activity analysis revealed a Pt mass-based activity of about 0.4 A mg$_{Pt}^{-1}$ at 900 mV cell voltage for the de-alloyed and ion-exchanged Pt–Cu catalysts, compared to 0.1 A mg$_{Pt}^{-1}$ and 0.15 A mg$_{Pt}^{-1}$ for the 30 wt% and the 45 wt% catalysts at 900 mV.

In essence, our MEA study proved how crucial a Cu-ion removal is to unfold the full potential of the Pt–Cu cathode catalyst concept.

3.4. Morphology and composition of de-alloyed MEAs

To gain insight in the migration processes and exact location of Cu ions during and after in situ de-alloying, a number of MEAs were activated by in situ de-alloying and the activation was stopped at various stages. Fig. 4 shows a SEM micrograph (Fig. 4a) and the Pt and Cu map (Fig. 4b and c) of the cross-section of a MEA at the beginning of the de-alloying protocol. The anode layer is the bright band on the left of Fig. 4a while the cathode layer with a $Pt_{25}Cu_{75}$ precursor electrocatalyst appears bright on the right of Fig. 4a. The Cu mapping in Fig. 4b clearly shows that large amount of Cu has accumulated inside the membrane in two diffuse "Cu bands" which are located closer to the cathode layer. Interestingly, the data in Fig. 4b also reveals a thin straight Cu band near the anode of the MEA. This suggests that some Cu ions did migrate all across the membrane, possibly already during the time of the MEA preparation. The elemental mapping cannot reveal the oxidation state of
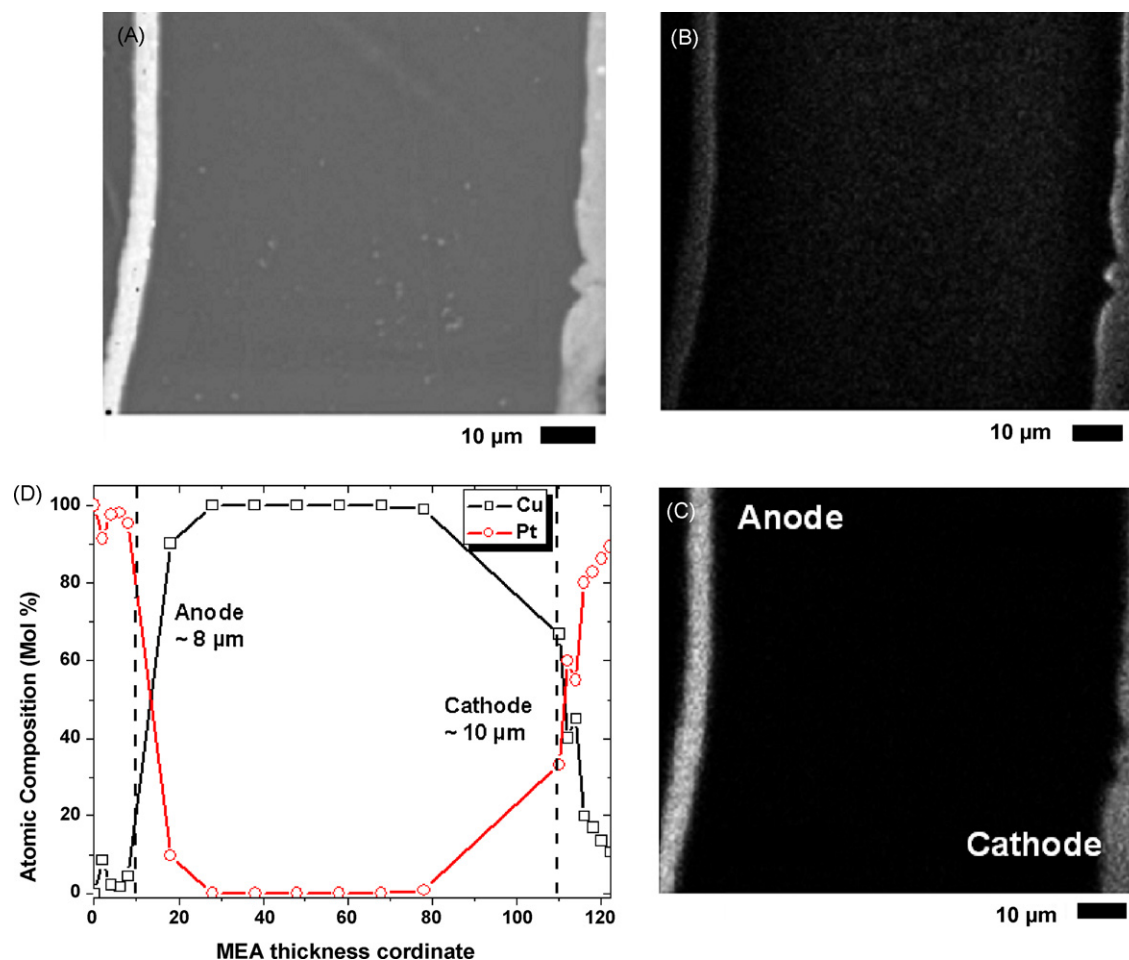
Fig. 5. EPMA mapping of an electrochemically in situ de-alloyed MEA where $Pt_{25}Cu_{75}$ was used as precursor on the cathode. Other conditions as in Fig. 5. (A) Backscattered image of the membrane cross-section, (B) Cu map of the MEA, (C) Pt map of the MEA and (D) atomic composition of PtCu across the MEA. *Note*: only in the simultaneous presence of Pt and Cu are the compositional values accurate. In the absence of one of the two species, the normalization displays the composition of the respective other as 100%. Catalyst loadings $L_{Pt,Cathode} = 0.2026\,mg_{Pt}\,cm^{-2}$ and $L_{Pt,Anode} = 0.1959\,mg_{Pt}\,cm^{-2}$.

the Cu inside the membrane; however, from optical inspection of the dissembled MEA a reddish color suggested the presence of at least some metallic Cu inside the membrane. Fig. 4c confirms that Pt is present on both electrode, and completely absent inside the membrane. Fig. 4d, finally reports the relative atomic Pt-to-Cu composition across the MEA. Note that we report normalized atomic weight composition, that is, if either Pt or Cu is absent, the respective other element is reported with 100 at.%. While the inside of the anode layer is pure Pt, a Cu band consisting of about 80 at.% Cu is located at the interface of anode layer and membrane. The inside of the membrane is Pt free, yet contains Cu. Due to the normalization of the compositional Pt:Cu data the reported Cu composition in Fig. 4d is at 100 at.%. The actual Cu composition inside the membrane cannot be accurately reported. Near the interface between membrane and cathode layer the Pt composition rises sharply to values between 50 at.% and 80 at.% inside the cathode layer.

After complete de-alloying, the elemental mapping reveals a different picture shown in Fig. 5. The broad Cu bands inside the membrane from Fig. 5b disappeared after de-alloying, while a thin Cu band near the anode remained visible (Fig. 5b). The Pt mapping (Fig. 5c) is essentially unchanged. The elemental mapping of Fig. 5d reveals that Cu remained inside the membrane with Pt being absent. The composition of the cathode layer now exhibits a distinct

spatial gradient with $Pt_{60}Cu_{40}$ near the interface to the membrane, and $Pt_{90}Cu_{10}$ near the interface of cathode layer and gas diffusion layer.

Interestingly, the membrane diameter was found to be larger after de-alloying (Fig. 5d compared to Fig. 4d) suggesting some swelling during the de-alloying protocol.

Ion exchange resulted in a compositional picture reported in Fig. 6. Fig. 6a shows significant bending of the MEA layers and evidenced significant mechanical stress on the MEA during the entire de-alloying protocol. The Cu mapping in Fig. 6b suggests that Cu atoms are present in the cathode layer. The weak Cu contrast inside the anode layer of Fig. 6b was unexpected and has remained unexplained to date. It is inconsistent with the EDX compositional data which suggest negligible amount of Cu in the anode and membrane. The Pt elemental mapping in Fig. 6c suggests Pt in the anode and cathode and a largely Pt-free membrane. However, at around $65–75\,\mu m$ from the left edge of the image some finite Pt atoms were detected suggesting Pt leaching/migration from the cathode into the membrane. The cathode layer composition now ranges from $Pt_{90}Cu_{10}$ at the inside of the cathode layer to almost pure Pt on the outside. Fig. 6d impressively demonstrates the effectiveness of the Cu-ion removal from the membrane by ion exchange using liquid acids. Except for the cathode layer, no significant Cu atoms
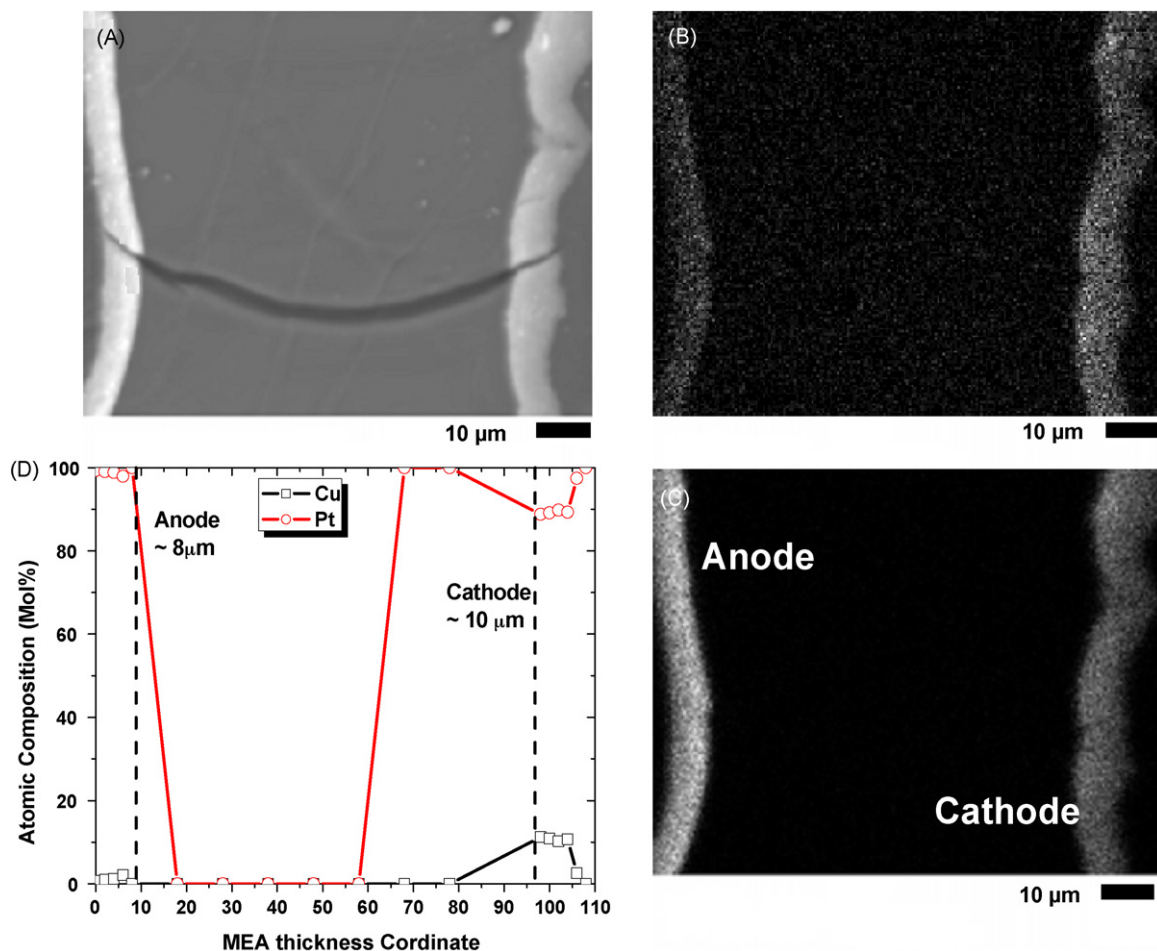
Fig. 6. EPMA mapping of an electrochemically in situ de-alloyed and ion-exchanged MEA with $Pt_{25}Cu_{75}$ used as precursor on the cathode. Other conditions as in Fig. 5. (A) Backscattered image of the membrane cross-section, (B) Cu map of the MEA, (C) Pt map of the MEA and (D) atomic composition of PtCu throughout the cross-section. *Note*: only in the simultaneous presence of Pt and Cu are the compositional values accurate. In the absence of one of the two species, the normalization displays the composition of the respective other as 100%. Catalyst loadings $L_{Pt,Cathode} = 0.2026$ mg_{Pt} cm^{-2} and $L_{Pt,Anode} = 0.1959$ mg_{Pt} cm^{-2}.

remained inside the MEA, ensuring acceptable ionic conductivities and MEA performances.

4. Conclusions

We have investigated the voltammetric, morphological, compositional and crystallographic changes that occurred during the in situ de-alloying of a MEA employing a carbon-supported $Pt_{25}Cu_{75}$ alloy nanoparticle precursor at the cathode. From our experimental observations we can conclude:

(1) The X-ray diffraction patterns as well as the cyclic voltammetric profiles before and after de-alloying are consistent with the removal of large amount of Cu atoms from the cathode precursor catalyst. Non-alloyed pure Cu as well as a portion of the Cu inside the bimetallic phase disappears.
(2) The lattice constant of he Pt–Cu alloy phase increases in the de-alloying process, possibly leading to compressive lattice strain in the relaxation process.
(3) The de-alloyed catalysts exhibit voltammetric responses that closely resemble those of pure Pt indicating the absence of Cu on the surface in the activated state.
(4) The MEA performance of de-alloyed MEAs without ion exchange is very low evidencing the detrimental nature of metal dissolution from catalysts.

(5) The Pt mass-based performance of de-alloyed and ion-exchanged Pt–Cu cathodes is significantly higher than pure Pt cathodes (0.4 A mg_{Pt}^{-1} at 900 mV compared to 0.1 A mg_{Pt}^{-1} for a 45 wt% Pt/C standard).
(6) Elemental mapping of de-alloyed MEAs revealed that large amount of Cu ions are trapped inside the membrane of the MEA already before de-alloying due to the leaching of the acidic ink formulation. More Cu is de-alloyed during the de-alloying process into the membrane. Some Cu appears to migrate to the anode layer.
(7) EPMA further showed that ion exchange is an effective means to remove Cu ions from the membrane.

References

[1] S. Koh, P. Strasser, J. Am. Chem. Soc. 129 (2007) 12624–12625.
[2] R. Srivastava, P. Mani, N. Hahn, P. Strasser, Angew. Chem. Int. Ed. 46 (2007) 8988–8991.
[3] W. Vielstich, A. Lamm, H. Gasteiger (Eds.), Handbook of Fuel Cells—Fundamentals, Technology, and Applications, Wiley, Chichester, UK, 2003.
[4] H.A. Gasteiger, S.S. Kocha, B. Sompalli, F.T. Wagner, Appl. Catal. B: Environ. 56 (2005) 9–35.
[5] V.R. Stamenkovic, B.S. Mun, K.J.J. Mayrhofer, P.N. Ross, N.M. Markovic, J. Am. Chem. Soc. 128 (2006) 8702–8988.
[6] V. Stamenkovic, B.S. Moon, K.J. Mayerhofer, P.N. Ross, N. Markovic, J. Rossmeisl, J. Greeley, J.K. Norskov, Angew. Chem. Int. Ed. 45 (2006) 2897–2901.
[7] V. Stamenkovic, T.J. Schmidt, P.N. Ross, N.M. Markovic, J. Electroanal. Chem. 554 (2003) 191–199.
[8] N.M. Markovic, P.N. Ross, Surf. Sci. Rep. 45 (2002) 117.
[9] V. Stamenkovič, T.J. Schmidt, P.N. Ross, N.M. Markovic, J. Phys. Chem. B 106 (2002) 11970–11979.
[10] U.A. Paulus, A. Wokaun, G.G. Scherer, T.J. Schmidt, V. Stamenkovic, N.M. Markovic, P.N. Ross, Electrochim. Acta 47 (2002) 3787–3798.
[11] U.A. Paulus, A. Wokaun, G.G. Scherer, T.J. Schmidt, V. Stamenkovic, V. Radmilovic, N.M. Markovic, P.N. Ross, J. Phys. Chem. B 106 (2002) 4181–4191.
[12] N.M. Markovic, T.J. Schmidt, V. Stamenkovic, P.N. Ross, Fuel Cells 1 (2001) 105.
[13] N.M. Markovic, P.N. Ross, CATTECH 4 (2000) 110–126.
[14] R.R. Adzic, J. Zhang, K. Sasaki, M.B. Vukmirovic, M. Shao, J.X. Wang, A.U. Nilekar, M. Mavrikakis, J.A. Valerio, F. Uribe, Top. Catal. 46 (2007) 249–262.
[15] M.B. Vukmiovic, J. Zhang, K. Sasaki, A.U. Nilekar, F. Uribe, M. Mavrikakis, R.R. Adzic, Electrochim. Acta 52 (2007) 2257–2263.
[16] K. Sasaki, J.X. Wang, M. Balasubramanian, J. McBreen, F. Uribe, R.R. Adzic, Electrochim. Acta 49 (2004) 3873.
[17] J. Zhang, Y. Mo, M. Vukmirovic, R. Klie, K. Sasaki, R. Adzic, J. Phys. Chem. B 108 (2004) 10955–10964.
[18] S.R. Brankovic, J.X. Wang, R.R. Adzic, Electrochem. Solid-State Lett. 4 (2001) A217–A220.
[19] J. Zhang, F.H.B. Lima, M.H. Shao, K. Sasaki, J.X. Wang, J. Hanson, R.R. Adzic, J. Phys. Chem. B 109 (2005) 22701–22704.
[20] J.L. Zhang, M.B. Vukmirovic, K. Sasaki, A.U. Nilekar, M. Mavrikakis, R.R. Adzic, J. Am. Chem. Soc. 127 (2005) 12480–12481.
[21] V. Stamenkovic, B.S. Mun, M. Arenz, K.J.J. Mayerhofer, C.A. Lucas, G. Wang, P.N. Ross, N. Markovic, Nat. Mater. 6 (2007) 241.
[22] V.R. Stamenkovic, B. Fowler, B.S. Mun, G. Wang, P.N. Ross, C.A. Lucas, N.M. Markovic, Science 315 (2007) 493.
[23] P. Strasser, S. Koh, J. Greeley, Phys. Chem. Chem. Phys. 10 (2008) 3670–3683.
[24] C. Yu, S. Koh, J. Leisch, M.T. Toney, P. Strasser, Faraday Dis. 140, in press, doi:10.1039/b801586d.
[25] P. Mani, R. Srivastava, P. Strasser, J. Phys. Chem. C 112 (2008) 2770–2778.
[26] P. Strasser, S. Koh, C. Yu, ECS Trans. 11 (2007) 167–180.
[27] Z. Liu, S. Koh, C. Yu, P. Strasser, J. Electrochem. Soc. 154 (2007) B1192–B1199.
[28] P. Mani, R. Srivastava, P. Strasser, ECS Trans. 11 (2007) 933–940.
[29] S. Koh, C. Yu, P. Strasser, ECS Trans. 11 (2007) 205–215.
[30] P. Strasser, unpublished, 2008.
[31] ICDD, Power Diffraction File (PDF). 2-Data CD, International Center for Diffraction Data—Power Diffraction File (PDF). 2-Data CD, 2002, http://www.icdd.com/.
[32] B.E. Warren, X-ray Diffraction, Dover Publications, Reading, MA, 1969.
[33] J. Friedel, Philos. Mag. 46 (1955) 514.
[34] L. Vegard, Zeitschrift fuer Physik 5 (1921) 2–26.
[35] V. Stamenkovic, N. Markovic, Langmuir 17 (2001) 2388–2394.
[36] N. Markovic, H.A. Gasteiger, P.N. Ross, Langmuir 11 (1995) 4098–4108.
[37] N. Markovic, P.N. Ross, Langmuir 9 (1993) 580–590.